

GEM-MACH-PAH: a new high-resolution chemistry transport model for North American PAHs
and benzene

Cynthia H. Whaley, Elisabeth Galarneau, Paul A. Makar, Ayodeji Akingunola, Wanmin
Gong, Sylvie Gravel, Michael D. Moran, Craig Stroud, Junhua Zhang, and Qiong Zheng

SUPPLEMENTAL MATERIAL

CONTENTS

Appendix A: Measurement Sites	2
Appendix B: Gas-particle partitioning analysis	6
B.1: Discussion of Junge-Pankow	6
B: Derivation of $m = -1$ for Junge-Pankow	8
B.2: Derivation of new K_{SW} for Dachs-Eisenreich scheme	9
Appendix C: Verification of PAH mobile EFs from other sources	11
Appendix D: Species-specific constants needed for scavenging	12
Appendix E: Call sequence of CHEM code for GEM-MACH-PAH	13
Appendix F: Additional Hamilton Analysis	14
References	15

Appendix A: Table of measurement sites

Table A.1: Benzene and PAH network measurement sites in the Pam Am model domain. The following codes are used in the “measurement” column: “PB”=PAHs and benzene measured; “justP”=only PAHs measured; “justB”=only benzene measured; and “wetdep”=wet deposition measured.

Note that NATTS have site IDs, but not names, therefore the first column provides the state where the particular site resides, and cities/towns were manually looked up and added for those sites that have PAH measurements.

Site name or State	Site ID	Latitude	Longitude	measurement
IADN sites				
University of Toronto, ON	UOT	43.8725	-79.18833	wetdep
St Clair, ON	STC	42.53594	-82.38978	wetdep
Burlington, ON	BUR	43.36889	-79.87028	wetdep
Burnt Island, ON	BNT	45.82833	-82.94806	justP
Point Petre, ON	PPT	43.84278	-77.15361	justP/wetdep
Sturgeon Point, NY	STP	42.69306	-79.055	justP/wetdep
Cleveland, OH	CLV	41.49214	-81.67853	justP/wetdep
Sleeping Bear Dunes, MI	SBD	44.76111	-86.0586	justP
Chicago IIT, IL	IIT	41.83444	-87.6247	justP
NAPS sites				
College and South, Windsor, ON	60211	42.29289	-83.0731	PB
Gage Institute, Toronto, ON	60427	43.65822	-79.3972	PB
Etobicoke South (Toronto Kipling), ON	60435	43.61076	-79.5219	PB
Elgin and Kelly, Hamilton, ON	60512	43.25778	-79.8617	PB
Experimental Farm, Simcoe, ON	62601	42.8569	-80.2703	PB
Egbert, ON	64401	44.23111	-79.7831	PB
Point Petre, ON	64601	43.84278	-77.1536	PB
Burnt Island, ON	65501	45.82833	-82.9481	PB
NATTS sites				
Middletown, OH	390170003	39.4938	-84.3543	justB
OH	390350038	41.47701	-81.6824	justB
OH	390350068	41.45478	-81.6344	justB
OH	390350069	41.519	-81.6378	justB
OH	390350071	41.49251	-81.67	justB
OH	390490034	40.00274	-82.9944	justB
OH	390515502	41.55002	-84.1365	justB
OH	390610014	39.19433	-84.479	justB
OH	390610044	39.13837	-84.7116	justB
OH	390610045	39.17093	-84.5287	justB

OH	390610046	39.11412	-84.5363	justB
OH	390810017	40.36644	-80.6156	justB
Ironton, OH	390875503	38.51814	-82.6688	PB
Franklin Furnace, OH	391450020	38.60934	-82.8225	PB
Franklin Furnace, OH	391450021	38.60066	-82.8296	PB
Franklin Furnace, OH	391450022	38.58808	-82.8348	PB
Warren, OH	391555504	41.23506	-80.8127	PB
MI	260330901	46.49361	-84.3642	justB
MI	261110951	43.60917	-84.2106	justB
MI	261110953	43.59139	-84.2094	justB
MI	261110955	43.58944	-84.2211	justB
MI	261110959	43.57419	-84.3216	justB
MI	261630015	42.30279	-83.1065	justB
Dearborn, MI	261630033	42.30754	-83.1496	PB
MI	261635502	42.35059	-83.0524	just B
Liberty, PA	420030064	40.32377	-79.8681	PB
Clairton, PA	420033007	40.29434	-79.8853	PB
Kennedy Township, PA	420035503	40.49435	-80.0964	PB
PA	420450002	39.83556	-75.3725	justB
PA	420710007	40.04667	-76.2833	justB
PA	420770004	40.61194	-75.4325	justB
PA	420910005	40.19255	-75.4575	justB
PA	421010004	40.00889	-75.0978	justB
PA	421010014	40.04962	-75.2408	justB
PA	421010047	39.94465	-75.1652	justB
PA	421010055	39.92287	-75.1869	justB
PA	421010063	39.88294	-75.2197	justB
PA	421010136	39.9275	-75.2228	justB
PA	421190001	40.95517	-76.8819	justB
PA	421250005	40.14667	-79.9022	justB
PA	420010001	39.92002	-77.3097	justB
PA	420030031	40.44337	-79.9903	justB
Philadelphia, PA	421010449	39.9825	-75.0831	justP
Buffalo, NY	360291013	42.98844	-78.9186	PB
Rochester, NY	360551007	43.1462	-77.5481	PB
NY	360050133	40.8679	-73.8781	justB
NY	360095501	42.08506	-78.4336	justB
NY	360291007	42.7273	-78.8498	justB
NY	360291014	42.99813	-78.8993	justB
NY	360310003	44.39308	-73.8589	justB
NY	360470118	40.69545	-73.9277	justB
NY	360610115	43.84955	-79.9357	justB

NY	360632008	43.08218	-79.0011	justB
NY	360810124	40.73614	-73.8216	justB
NY	360831003	42.73194	-73.6891	justB
NY	360850111	40.58027	-74.1983	justB
NY	360850132	40.58056	-74.1518	justB
NY	361030009	40.82799	-73.0575	justB
New York, NY	360050110	40.81616	-73.9021	PB
CT	90019003	41.11833	-73.3367	justB
CT	90031003	41.78472	-72.6317	justB
CT	90090027	41.3014	-72.9029	justB
DE	100031008	39.5778	-75.6107	justB
DE	100032004	39.73944	-75.5581	justB
NJ	340155501	39.83709	-75.244	justB
NJ	340210005	40.28309	-74.7427	justB
NJ	340230006	40.47282	-74.4224	justB
NJ	340230011	40.46218	-74.4294	justB
NJ	340273001	40.78763	-74.6763	justB
NJ	340390004	40.64144	-74.2084	justB
NJ	340395502	40.65205	-74.1999	justB
MD	240053001	39.31083	-76.4744	justB
MD	240330030	39.05528	-76.8783	justB
MD	245100006	39.34056	-76.5822	justB
MD	245100040	39.29806	-76.6047	justB
Washington, DC	110010043	38.92185	-77.0132	PB
Providence, RI	440070022	41.80795	-71.415	PB
RI	440030002	41.61524	-71.72	justB
RI	440070026	41.87467	-71.38	justB
RI	440071010	41.84157	-71.3608	justB
NH	330110020	42.99578	-71.4625	justB
NH	330111011	42.71866	-71.5224	justB
NH	330115001	42.86175	-71.8784	justB
NH	330150014	43.07533	-70.748	justB
MA	250092006	42.47464	-70.9708	justB
MA	250130008	42.19438	-72.5551	justB
MA	250213003	42.21177	-71.114	justB
MA	250250041	42.31737	-70.9684	justB
Boston, MA	250250042	42.32944	-71.0825	PB
Northbrook, IL	170314201	42.14	-87.7992	PB
O'Hare airport, Chicago, IL	170313103	41.96519	-87.8763	justB
Underhill, VT	500070007	44.52839	-72.8688	PB
VT	500070014	44.4762	-73.2106	justB
VT	500210002	43.60806	-72.9828	justB

East Chicago, IN	180895503	41.64921	-87.4475	PB
Gary, IN	180895504	41.5997	-87.3443	PB
IN	180190009	38.27668	-85.7638	justB
IN	180855502	41.23898	-85.8321	justB
IN	180890022	41.60668	-87.3047	justB
IN	180890023	41.65274	-87.4396	justB
IN	180890030	41.6814	-87.4947	justB
IN	180970078	39.8111	-86.1145	justB
IN	180970084	39.75885	-86.1154	justB
IN	181270024	41.61756	-87.1993	justB
IN	181570008	40.43164	-86.8525	justB
IN	181630016	37.97444	-87.5323	justB
Follansbee, WV	540095501	40.33564	-80.5953	PB
WV	540390010	38.3456	-81.6283	justB
WV	540610003	39.64937	-79.9209	justB
WV	540690010	40.11488	-80.701	justB
Richmond, VA	510870014	37.55655	-77.4004	PB
VA	510330001	38.20087	-77.3774	justB
VA	510590030	38.77335	-77.1047	justB
VA	516700010	37.28962	-77.2918	justB
VA	518100008	36.84188	-76.1812	justB
OH	391450020	38.60934	-82.82251	N/A
OH	391450021	38.60066	-82.82964	N/A

Appendix B: Gas-particle partitioning analysis

Appendix B.1 Junge-Pankow partitioning description and why it wasn't used in GEM-MACH-PAH

Junge-Pankow partitioning (JP) is based on Langmuir adsorption (Langmuir, 1918). It expresses partitioning as a particulate fraction ϕ_k for each PAH species, k:

$$\phi_k = \frac{c\theta}{p_{L,k}^o + c\theta} \quad , \quad (\text{B.1.1})$$

where ϕ_k is equal to the particulate concentration divided the total PAH species concentration. When $\phi_k = 1$, all of the concentration is in the particle phase, and none is in the gas phase, while $\phi_k = 0$ means all of the PAH is in the gas phase. θ is the total dry aerosol-particle surface area (m^2), which are treated as spherical, $p_{L,k}^o$ is the subcooled liquid saturated vapor pressure per PAH species, and c is a constant that depends on the PAH species and the temperature (Junge, 1977).

The vapor pressure is calculated using the relation:

$$\log K_{p,k} = m_K \log p_{L,k}^o + b_K \quad (\text{B.1.2})$$

where $m_{p,k}$ and $b_{p,k}$ come from Offenberg and Baker (1999)'s supporting information for PAHs.

Figure B.1b shows sample plots of ϕ_k vs $\log p_{L,k}^o$. These examples show how the measurements (blue crosses) differ from the JP model (purple points and black line), which requires that $m_K = -1$ (see next section for the derivation of this). The JP formulation does not allow for improvement given the $m_K = -1$ constraint. Therefore, the Dachs-Eisenreich formulation is examined next.

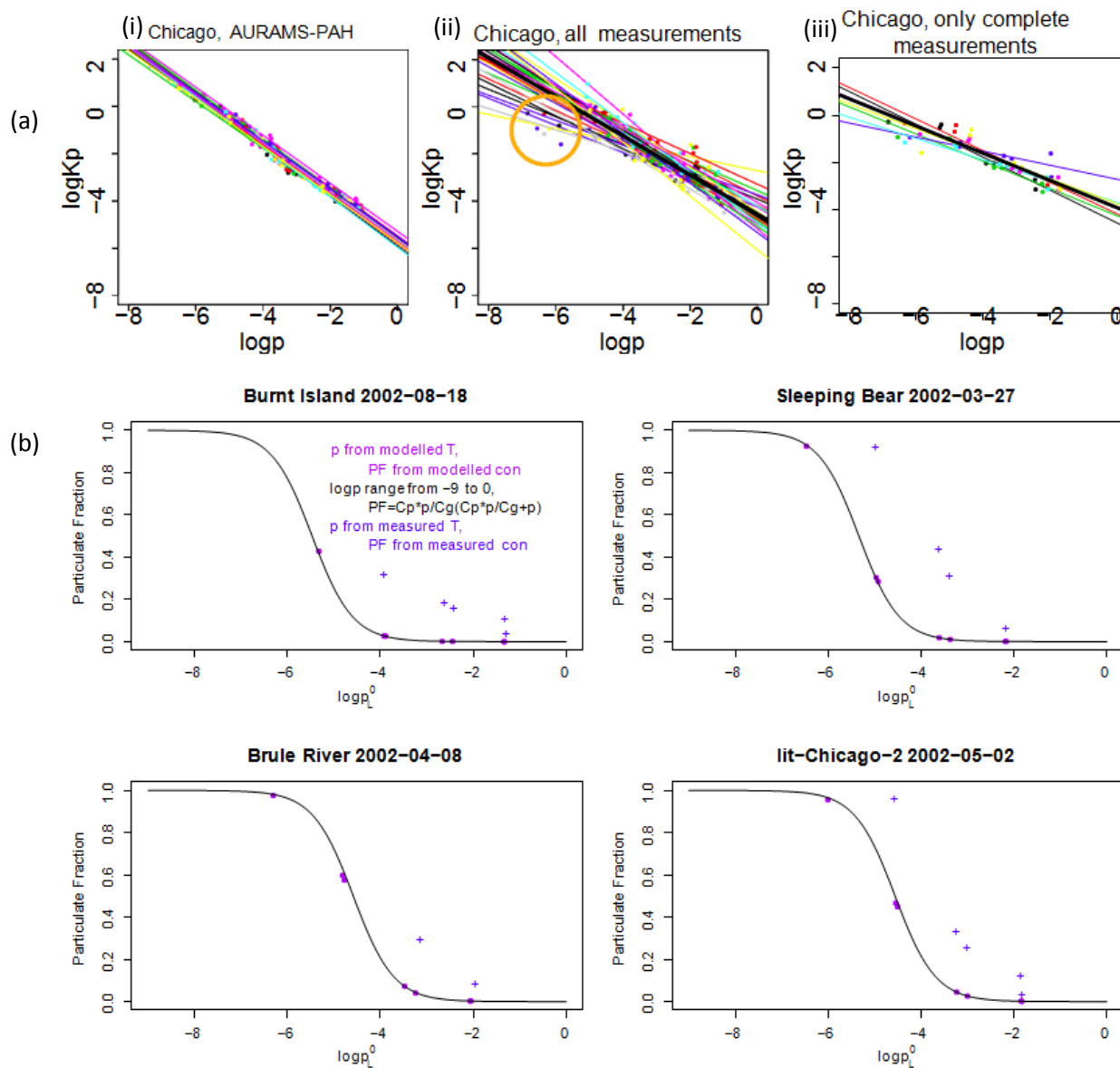


Figure B.1: (a) Chicago (taken as example) modelled (from AURAMS-PAH) and measured $\log Kp$ vs $\log p^\circ$ for all 7 PAHs, and their linear fits for 2002 data. Thick black line indicates the median linear fit. a(i) original JP and DE partitioning scheme, a(ii) all measurements, a(iii): only those measurements where all 7 PAHs were measured. (b) Particulate fraction (ϕ) vs $\log p_L^\circ$ for AURAMS-PAH model and 2002 measurement samples from four sites. The Junge-Pankow model is shown for 7 PAH species in purple points, and Eq. (B.1.1) as a black line. The measurements are shown as blue crosses.

Appendix B: Derivation of $m = -1$ for JP formulation, starting with Eq. (B.1.1)

Junge-Pankow relationship:

$$\phi = \frac{C_p}{C_p + C_g} = \frac{c\theta}{c\theta + p_L^\circ} \quad (\text{B1})$$

$$\frac{C_p + C_g}{C_p} = \frac{c\theta + p_L^\circ}{c\theta} \quad (\text{B2})$$

$$1 + \frac{C_g}{C_p} = 1 + \frac{p_L^\circ}{c\theta} \quad (\text{B3})$$

$$\frac{C_g}{C_p} = \frac{p_L^\circ}{c\theta} \quad (\text{B4})$$

$$\frac{C_p}{C_g} = \frac{c\theta}{p_L^\circ} \quad (\text{B5})$$

$$(\text{B6})$$

But,

$$\theta = C_{SSA} \left(\frac{m^2}{\mu g} \right) C_{TSP} \left(\frac{\mu g}{m^3} \right) \quad (\text{B7})$$

Subbing in:

$$\frac{C_p}{C_g} = \frac{cC_{SSA}C_{TSP}}{p_L^\circ} \quad (\text{B8})$$

$$\frac{C_p/C_{TSP}}{C_g} = K_p = \frac{cC_{SSA}}{p_L^\circ} \quad (\text{B9})$$

$$(\text{B10})$$

Take log of both sides:

$$\log \left(\frac{C_p/C_{TSP}}{C_g} \right) = \log(cC_{SSA}) - \log(p_L^\circ) \quad (\text{B11})$$

$$= -1 \log(p_L^\circ) + \log(cC_{SSA}) \quad (\text{B12})$$

Thus, for JP to be in a format that fits $\log K_p = m \log p_L^\circ + b$, m can only be -1 .

Appendix B.2: How the Dachs-Eisenreich parameters were changed based on empirical evidence

The Dach-Eisenreich expression for K_p is:

$$\begin{aligned} K_{p,k} &= 10^{-12} \left(\frac{1.5 f_{OC}}{\rho_{oct}} K_{OA,k} + f_{EC} K_{SA,k} \right) \\ &= 10^{-12} f_{EC} K_{SA,k} + 1.5 \times 10^{-12} \frac{f_{OC}}{\rho_{oct}} K_{OA,k} \end{aligned} \quad (\text{B.2.1})$$

where f_{OC} and f_{EC} are the organic and elemental carbon fractions respectively, ρ_{oct} is the density of octanol, the octanol-air partitioning coefficient, $K_{OA,k}$, is related to temperature:

$$K_{OA,k} = 10^{\frac{m_{OA,k}}{T} + b_{OA,k}} \quad (\text{B.2.2})$$

where $m_{OA,k}$ and $b_{OA,k}$ are taken from Odabasi et al (2006), and the soot-air partitioning coefficient, $K_{SA,k}$, is related to the soot-water and air-water partitioning coefficients:

$$\begin{aligned} K_{SA,k} &= K_{SW,k} e^{-K_{AW,k}} \\ &= K_{SW,k} e^{-\left(\frac{m_{AW,k}}{T} + b_{AW,k}\right)}, \end{aligned} \quad (\text{B.2.3})$$

where $m_{AW,k}$ and $b_{AW,k}$ are from Sander (1999) and Bamford et al (1999). An update for $b_{AW,k}$ was calculated from the 25°C $K_{AW,k}$ values given in Ma et al (2010) using Eq. (B.2.3). $K_{OA,k}$ and ρ_{oct} are also well-known, and make the second term in Eq. (B.2.1) four orders of magnitude smaller than the first term. The $K_{SW,k}$ values (in Eq. (B.2.3)) are highly uncertain. Using our new AURAMS-PAH model-measurement comparisons, we have determined new $K_{SW,k}$ values that would improve the DE particulate fraction representation.

Fig. B.1a shows $\log K_{p,k}$ vs $\log p_{L,k}$ for each 2002 Chicago measurement sample (of multiple PAH species) in the Galarneau et al (2014) study (these are measurements of up to 7 PAH species in the gas and particle phases, thus for each PAH, the gas-particle partitioning coefficient (K_p can be plotted against that PAH's vapour pressure), and their linear fits. Eq. (B.1.2) governs the data relationship, but the observations have more spread in slope than the AURAMS-PAH model is capable of representing (shown in Figure B.1a). Using the JP or DE formulation, the model can not represent the variability in the slope, however, unlike the JP formulation, the DE model slope (m_K) can be altered to better match observations. The modeled slope, at -1, was too steep compared to the measurements (Fig. B.1a (i) vs. (ii) and (iii)). Note that most of the measured samples did not have BaP measurements, as this species is difficult to measure unless its concentrations are high. Therefore, the median line from the fits that include all samples (thick

black line in Fig. B.1a(ii)) does not represent BaP measurements well. BaP points tend to fall well below the median line (see circle in Fig. B.1a(ii)). Therefore, we selected only samples that had all seven PAHs measured (from all sites -- shown in Fig. B.1a(iii) for Chicago samples), and calculated a median line from these linear fits. This median line better represents the slope and intercept of all PAHs, including BaP. Chicago was shown as an example, however, the original modelled slopes for all sites were too steep (too negative), and the intercepts too low.

Therefore, to adjust $K_{SW,k}$, we utilize the median m_k and b_k from the 2002 North American measurements, described above. First, we substitute Eq. (B.1.2) into Eq. (1) to get:

$$\begin{aligned}\log K_{p,k} &= m_K \left(\frac{m_{p,k}}{T} + b_{p,k} \right) + b_K \\ &= \frac{m_K m_{p,k}}{T} + m_K b_{p,k} + b_K\end{aligned}\quad (\text{B.2.4})$$

Fig. 2a shows the all-site (2002) ensemble of AURAMS-PAH model-over-measured $\log K_p$ and (b) particulate fraction, in green. The "adjusted model" -- which is actually just a recalculation of $\log K_p$ from Eq. (B.2.4), using AURAMS-PAH temperature and the median measured m_K and b_K -- is plotted in purple.

We then substitute Eq. (B.2.3) into Eq. (B.2.1), dropping the second term in equation (B.2.1) because we have verified that it is negligible, and because doing so greatly simplifies the math, to get:

$$K_{p,k} = 10^{-12} f_{EC} K_{SW,k} e^{-\left(\frac{m_{AW,k}}{T} + b_{AW,k}\right)} \quad (\text{B.2.5})$$

We set the right-hand-side of Eq. (B.2.4) equal to the log of $K_{p,k}$ from Eq. (B.2.5) to get our new $K_{SW,k}$ expression:

$$K_{SW,k} = \frac{10^{\left(\frac{m_K m_{p,k}}{T} + m_K b_{p,k} + b_K + 12\right)}}{f_{EC} e^{-\left(\frac{m_{AW,k}}{T} + b_{AW,k}\right)}} \quad (\text{B.2.6})$$

Eq. (B.2.6) is thus a means of describing PAH partitioning based on measurements, and the resulting $K_{SW,k}$ values are summarized in Table 1. The new $K_{SW,k}$ values will go into equation B.2.3 to give new $K_{SA,k}$ values that will go into equation B.2.1, which does the PAH partitioning in the model.

Appendix C: Verification of PAH mobile EFs from literature and SPECIATE sources

We require total PAH (gas + particle phases) emissions for our model, however about half of the compiled EFs (from the literature and from SPECIATE) only reported EFs for the particulate component of total PAH. Therefore, the EFs from those studies could not be used. The remaining SPECIATE data contained values that were sometimes unrealistically high (e.g., up to 20% phenanthrene in the TOG mass, which is orders of magnitude larger than typical values), and the relevant databases and reports lacked explanations for these anomalies. Therefore, none of the SPECIATE EFs were used in our determination of new PAH emissions.

From the remaining publications, the on-road EFs we recorded fell into the eight vehicle categories mentioned above (e.g., LDGV (Lim et al., 2007; de Abrantes et al., 2009); LDDV (Karavalakis et al., 2011); LDDT (Westerholm et al., 2001; Nelson et al., 2008); HDDV (Mi et al., 2000; Lim et al., 2005; Nelson et al., 2008); and MC (Yang et al., 2005; Spezzano et al., 2008)). When the EFs were converted to units of mass PAH per mass TOG for each of the vehicle classes, it was found that for some species/vehicle classes the EFs spanned up to two orders of magnitude within the same study, and up to three orders of magnitude across different studies. The EFs differ greatly within each category because the studies examined report on emissions from a variety of fuels (e.g., diesel can have varying percentages of biodiesel added), driving speeds (e.g., idling, city driving, highway driving, etc), and temperatures (e.g., cold start, cold outdoor temperatures, warm engine, etc.), whereas the TOG values that the PAHs were normalized to were only reported for different types of roads (e.g., urban, highway). When publications reported EFs for multiple fuel types, the most relevant EFs were kept (e.g., in Canada only ultralow sulfur diesel (ULSD), and unleaded gasoline fuels are used).

With these updated PAH EFs in hand, SMOKE was run to generate gridded emissions files of 28 usual GEM-MACH emitted species plus benzene and seven gas-phase PAHs on two model grids, a continental grid with 10-km horizontal grid spacing (Fig. 1a) and the "Pan Am" grid with 2.5-km grid spacing (Fig. 1b). We then ran the model with both the "recent-literature-based" EFs for eight vehicle classes (using the median value in each category) and with MOVES 2014 EFs for just two classes (gasoline and diesel). The literature based EFs were generally higher than those from MOVES. The model biases for PAHs were smaller with the MOVES EFs in both Canada and the U.S., therefore, the model results we show in Section 4 are from the simulation with MOVES mobile emissions. We will discuss the results of the on-road mobile EFs further when we analyze the model output (Section 4.2.1).

Appendix D: Table of species-specific constants used in the model for dry and wet removal.

Table D.1: Species-specific constants used in the model for dry and wet scavenging.

Constant	Benzen e	PHEN	ANTH	FLRT	PYR	BaA	CHRY	BaP	Source
¹ α	0.05	0.1	0.1	0.2	0.2	0.2	0.2	0.3	Zhang et al (2015)
² β	0.1	0.3	0.3	0.4	0.4	0.5	0.5	0.6	Zhang et al (2015)
³ H* (unit)	22.7	22.7	20.2	70.1	76.8	146	227	91.1	Staudinger & Roberts (2001) for benzene. Ma et al. (2010) for PAHs
⁴ f_0 (unit)	0	0	0	0	0	0	0	0	NA
⁵ ats (K)	3950	4700	4000	6900	6900	4700	4700	2405	Sander (1999)
⁶ vap. pres. slope	-1211.03	-3706.04	-3710.87	-4081.11	-4153.89	-4563.27	-4577.21	-5046.88	Shiu and Ma (2000)
⁷ vap. pres. Int.	6.0299	11.42	11.42	11.59	11.62	11.81	11.82	12.04	Shiu and Ma (2000)

¹weights applied to resistance for SO₂ for a given gas

²weights applied to resistance for O₃ for a given gas

³Henry's law constant, solubility in water

⁴chemical reactivity, used to evaluate how much gas is dissolved in mesophyll

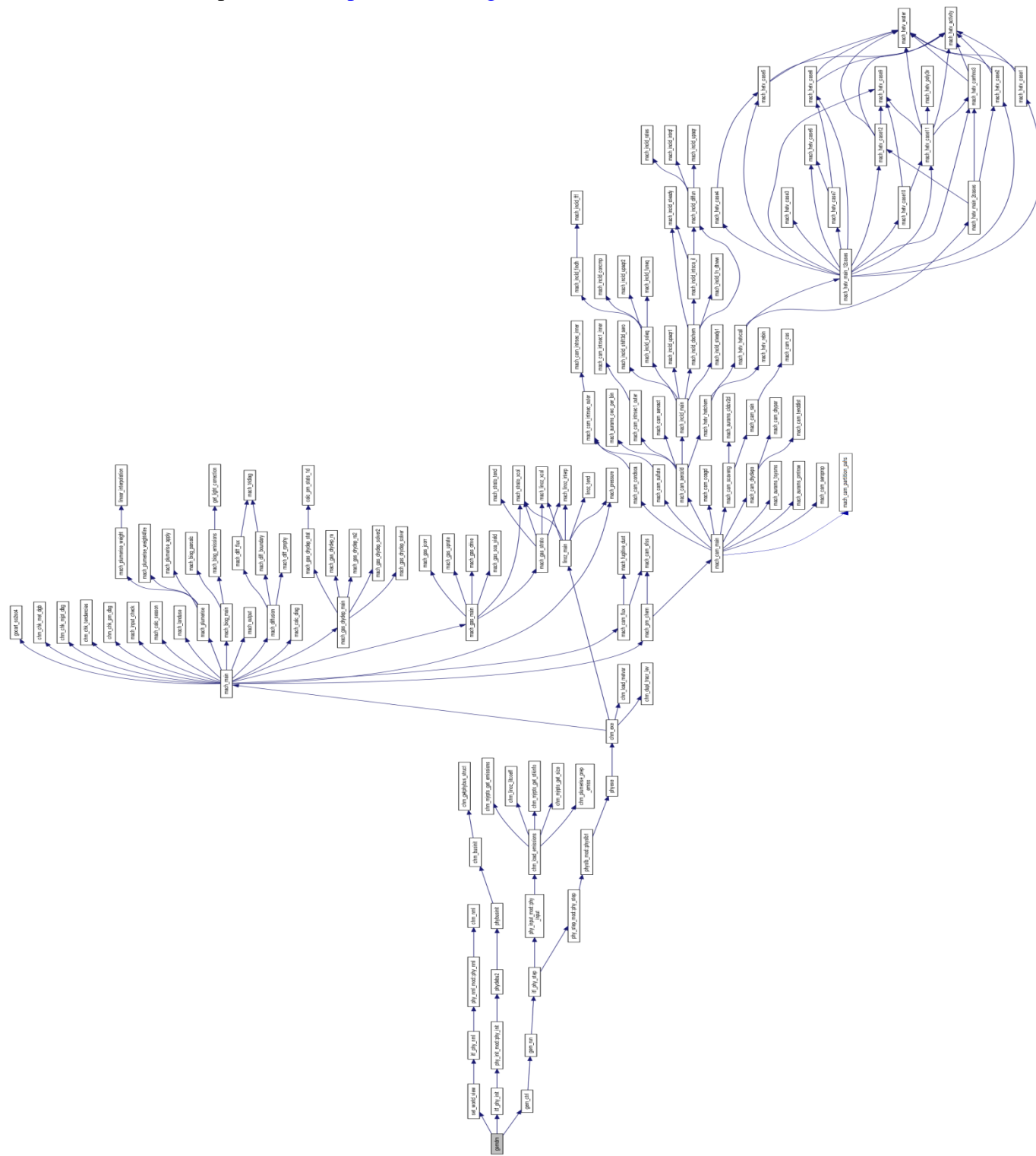
⁵temperature dependency for solubility

⁶sub-cooled liquid saturation vapour pressure (Pa), slope

⁷sub-cooled liquid saturation vapour pressure (Pa), intercept

Appendix E: Call sequence of MACH (chemistry) part of GEM-MACH-PAH model.

For the CHEM code, please see <https://zenodo.org/record/1162252#.Wt39IMZII-J>



Appendix F: Hamilton PAH_i/PM_{2.5} analysis

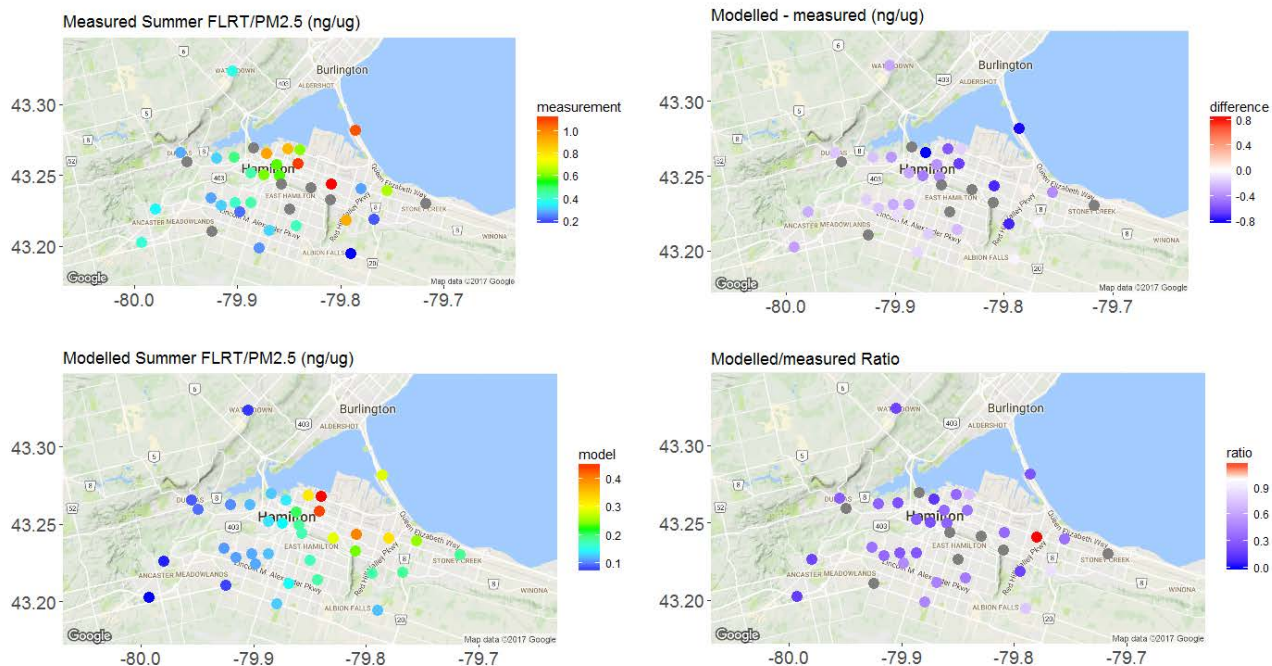


Figure F.1: Left: Measured and modelled and concentration ratios of FLRT/PM_{2.5} in Hamilton, Ontario for two-week summer 2009 period. Right: Their differences and ratios. Note that spatial pattern in model bias is missing.

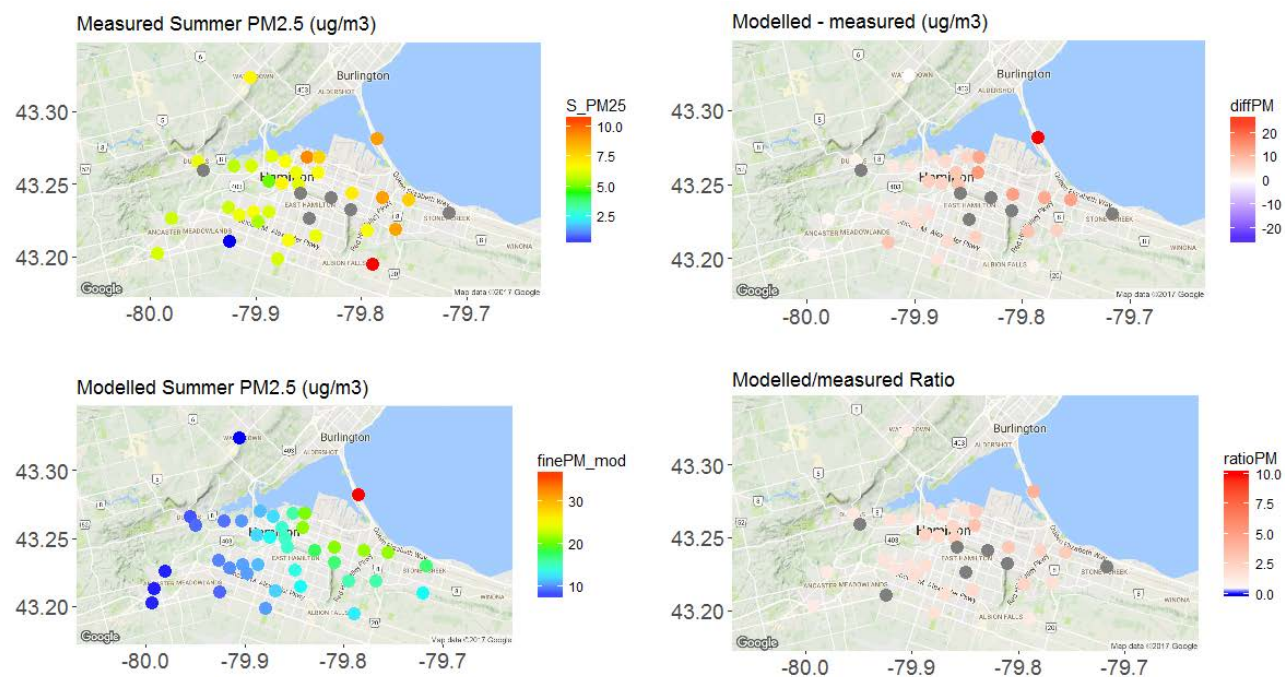


Figure F.2: Same as Fig. E.1, but for PM_{2.5} concentrations. Note that modelled PM_{2.5} is biased high, and is causing the spatial pattern seen in the PAH bias (cf. Fig. 4a).

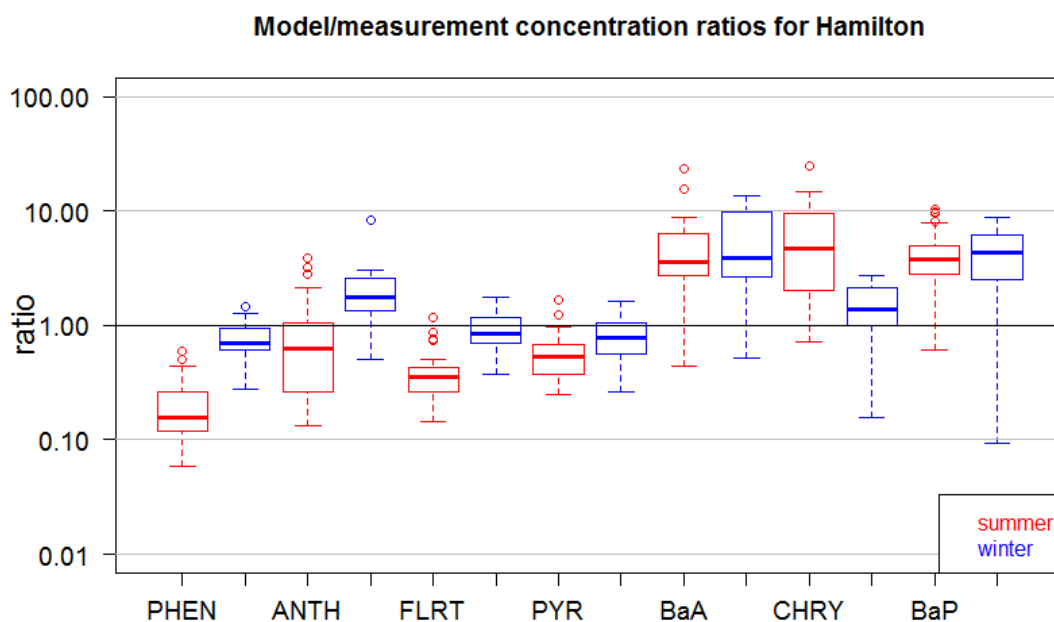


Figure F.3: Model/measurement ratios of PAH_i/PM_{2.5} in Hamilton (summer and winter). Note that all biases have shifted down compared to Fig. 5a because the modelled PM_{2.5} is biased high compared to measurements.

References

- Bamford, H. A., Poster, D. L., and Baker, J. E.: Temperature dependence of Henry's Law constants of thirteen polycyclic aromatic hydrocarbons between 4°C and 31°C, *Environ. Toxic. Chem.*, 18, 1905–1912, 1999.
- de Abrantes, R., de Assunção, J. V., Pesquero, C. R., Bruns, R. E., and Nóbrega, R. P.: Emission of polycyclic aromatic hydrocarbons from gasohol and ethanol vehicles, *Atmos. Environ.*, 43, 648–654, doi:10.1016/j.atmosenv.2008.10.014, 2009.
- Galarneau, E., Makar, P. A., Zheng, Q., Narayan, J., Zhang, J., Moran, M. D., Bari, M. A., Pathela, S., Chen, A., and Chlumsky, R.: PAH concentrations simulated with the AURAMS-PAH chemical transport model over Canada and the USA, *Atmos. Chem. Phys.*, 14, 4065–4077, doi:10.5194/acp-14-4065-2014, 2014.
- Junge, C. E.: Basic considerations about trace constituents in the atmosphere as related to the fate of global pollutants, in: *Fate of pollutants in the air and water environments*, edited by Suffet, I. H., pp. 7–25, Wiley, New York, 1977.
- Karavalakis, G., Boutsika, V., Stournas, S., and Bakeas, E.: Biodiesel emissions profile in modern diesel vehicles. Part 2: Effect of biodiesel origin on carbonyl, PAH, nitro-PAH and oxy-PAH emissions, *Sci. Tot. Environ.*, 409, 738–747, doi:10.1016/j.scitotenv.2010.11.010, 2011.

- Langmuir, I.: The adsorption of gases on plane surfaces of glass, mica, and platinum, *J. Am. Chem. Soc.*, 40, 1361–1402, 1918.
- Lim, M. C. H., Ayoko, G. A., Morawaska, L., Ristovski, Z. D., and Jayaratne, E. R.: Effect of fuel composition and engine operating conditions on polycyclic aromatic hydrocarbon emissions from a fleet of heavy-duty diesel buses, *Atmos. Environ.*, 39, 7836–7848, doi:10.1016/j.atmosenv.2005.09.019, 2005.
- Lim, M. C. H., Ayoko, G. A., Morawaska, L., Ristovski, Z. D., and Jayaratne, E. R.: Influence of fuel composition on polycyclic aromatic hydrocarbon emissions from a fleet of in-service passenger cars, *Atmos. Environ.*, 41, 150–160, doi:10.1016/j.atmosenv.2006.07.044, 2007.
- Ma, Y.-G., Lei, Y. D., Xiao, H., Wania, F., and Wang, W.-H.: Critical review and recommended values for the physical-chemical property data of 15 polycyclic aromatic hydrocarbons at 25°C, *J. Chem. Eng. Data*, 55, 819–825, doi:10.1021/je900477x, 2010.
- Mi, H.-H., Lee, W.-J., Chen, C.-B., Yang, H.-H., and Wu, S.-J.: Effect of fuel aromatic content on PAH emission from a heavy-duty diesel engine, *Chemosphere*, 41, 1783–1790, 2000.
- Nelson, P. F., Tibbett, A. R., and Day, S. J.: Effects of vehicle type and fuel quality on real world toxic emissions from diesel vehicles, *Atmos. Environ.*, 42, 5291–5303, doi:10.1016/j.atmosenv.2008.02.049, 2008.
- Odabasi, M., Cetin, E., and Sofuoglu, A.: Determination of octanol-air partition coefficients and supercooled liquid vapor pressures of PAHs as a function of temperature: application to gas-particle partitioning in an urban atmosphere, *Atmos. Environ.*, 40, 6615–6625, doi:10.1016/j.atmosenv.2006.05.051, 2006.
- Offenberg, J. H. and Baker, J. E.: Aerosol size distributions of polycyclic aromatic hydrocarbons in urban and over-water atmospheres, *Environ. Sci. Technol.*, 33, 3324–3331, doi:10.1021/es990089c, 1999.
- Sander, R.: Modeling atmospheric chemistry: interactions between gas-phase species and liquid cloud/aerosol particles, *Surveys in Geophysics*, 20, 1–31, 1999.
- Shiu, W.-Y., Ma, K.-C.: Temperature dependence of physical-chemical properties of selected chemicals of environmental interest. I. Mononuclear and polynuclear aromatic hydrocarbons, *J. Phys. Chem. Ref. Data*, 29, no. 1, 41-130, doi:10.1063/1.556055, 2000.
- Spezzano, P., Picini, P., Cataldi, D., Messale, F., and Manni, C.: Particle- and gas-phase emissions of polycyclic aromatic hydrocarbons from two-stroke, 50-cm³ mopeds, *Atmos. Environ.*, 42, 4332–4344, doi:10.1016/j.atmosenv.2008.01.008, 2008.
- Staudinger, J., Roberts, P. V.: A critical compilation of Henry's law constant temperature dependence relations for organic compounds, *Chemosphere*, 44, 561-576, doi:10.1016/S0045-6535(00)00505-1, 2001.
- Westerholm, R., Christensen, A., Törnqvist, M., Ehrenberg, L., Rannug, U., Sjögren, M., Rafter, J., Soontjens, C., Almén, J., and Grägg, K.: Comparison of exhaust emissions from Swedish environmental classified diesel fuel (MK1) and European program on emissions, fuels, and engine technologies (EPEFE) Reference fuel: a chemical and biological characterization, with viewpoints on cancer risk, *Environ. Sci. Technol.*, 35, 1748–1754, doi:10.1021/es000113i, 2001.
- Yang, H.-H., Chien, S.-M., Chao, M.-R., and Lin, C.-C.: Particle size distribution of polycyclic aromatic hydrocarbons in motorcycle exhaust emissions, *J. Haz. Mat.*, B125, 154–159, doi:10.1016/j.jhazmat.2005.05.019, 2005.
- Zhang, L., Cheng, I., Muir, D., Charland, J.-P.: Scavenging ratios of polycyclic aromatic compounds

in rain and snow in the Athabasca oil sands region, *Atmos. Chem. Phys.*, 15, 1421-1434, doi: 10.5194/acp-15-1421-2015, 2015.